

Chapter 4

Simulations

4.1 Introduction

In the previous chapter, a methodology has been developed that will be used to perform the control needed for actuator characterization. A study using this methodology allowed the investigation of the limitations that may be encountered while applying the controller experimentally. These limitations not only concern the operational range of the actuator used as a control actuator but also problems of resonance of the test bed itself. Therefore, before going any further into the process of developing the real time active controller, it may be worth spending some time creating different models that should give a better insight into problems that may arise in experiments.

First, a model of a stack actuator will be developed and applied to the theory of control to help draw some conclusions on controllability limitations. Then, a simulation method using experimental time history measurements from a preliminary test set-up will be considered. This simulation will also help to determine the control limitations.

4.2 Simulation Using a Model of the Actuator

4.2.1 Model of a stack actuator

As a preliminary study, a simple model of a stack actuator working against a load has been chosen to investigate the limitations of the control methodology developed in Chapter 3. A stack piezoelectric actuator is a strain device that stretches or contracts when a voltage (of appropriate polarity) is applied to it [27]. The stack actuator can be modeled as a force (called F_s) which acts in parallel to a spring and a damper. The force, F_s , is also called the blocked force. It represents the amount of force the actuator produces when sufficiently clamped on both sides such that there is no displacement. The stiffness (called K_s) of the spring models the internal stiffness of the actuator and the damper (whose damping coefficient is called C_s) models the structural damping of the actuator. As the actuator is allowed to strain, the force due to the spring and the damper act against the blocked force to reduce the overall force output (called F_m) of the actuator (Cf: Figure 4.1).

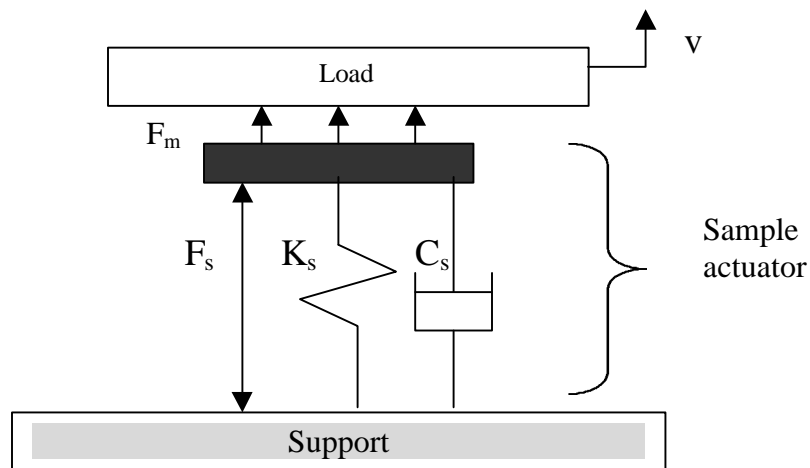


Figure 4.1: Model of stack actuator

Using a frequency domain formulation, the total force output of the actuator acting at a frequency, ω , is given by:

$$F_m = F_s + \frac{K_s v}{j\omega} + C_s v \quad (4.1)$$

Where v is the velocity of the load on top of the actuator (Cf: figure 4.1). The force and the velocity of the load are related to its own mechanical impedance. Using basic mechanics of material relationship [26] to express the internal stiffness in terms of parameters usually given for an existing stack actuator, a new expression for K is:

$$K = \frac{EA}{L} \quad (4.2)$$

where E is Young's modulus for the actuator, A is its cross-sectional area and L is its length.

For preliminary analysis, the structural damping coefficient, C , will be assumed to be proportional to the spring constant K with the following relationship:

$$C = K\eta/\omega \quad (4.3)$$

where η , also called structural damping factor, is a coefficient which is usually smaller than unity.(i.e. typically $\eta=0.1$ for a moderately damped system).

Finally, using equations developed for piezoelectric materials [27], an expression for the blocked force produced by the stack piezoelectric actuator used as the sample actuator can be obtained. As the longitudinal force and displacement of the actuator are the only parameters of interest, the blocked force will be equal to:

$$F_s = K_s d_{33s} S_s \quad (4.4)$$

where d_{33s} is a piezoelectric strain constant for the sample actuator and s_s is the electrical input (voltage) to the actuator.

Figure 4.2 shows a model of the complete system including both the sample and the control actuators (Cf: Figure 3.1).

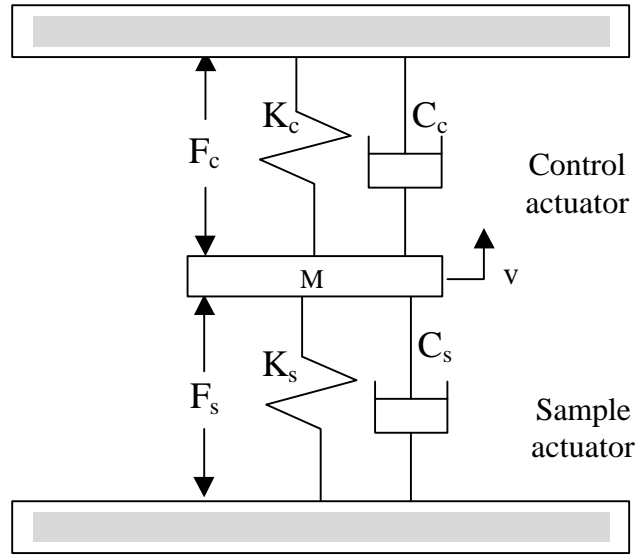


Figure 4.2: Dynamic model of the test apparatus

Applying Newton's second law to this system and assuming harmonic excitation at frequency ω , the equation of motion for the mass M is given by:

$$K_s d_{33_s} s_s - K_c d_{33_c} s_c = [w^2 M - (K_d + K_c) - jw(C_s + C_c)]w \quad (4.5)$$

where w is the vertical displacement. Using complex notation we assume a solution:

$$w(t) = Ae^{j\omega t} \quad (4.6)$$

where A is the complex amplitude of the displacement. Therefore, with a simple derivation, the expression for the corresponding velocity becomes:

$$v = \frac{dw(t)}{dt} = j\omega w. \quad (4.7)$$

As seen in Chapter 3, substituting equation (4.7) into equation (4.5), the velocity coefficients (velocity of the mass normalized to voltage input) due to the two different actuators acting separately (i.e.: $v = v_s + v_c$) can be expressed as:

$$v_s = \frac{-K_s d_{33_s} \mathbf{w}}{\mathbf{w}(C_c + C_s) + j[\omega^2 M - (K_s + K_c)]} \quad (4.8)$$

and

$$v_c = \frac{-K_c d_{33_c} \mathbf{w}}{\mathbf{w}(C_c + C_s) + j[\omega^2 M - (K_s + K_c)]}. \quad (4.9)$$

From equation (4.1), the same approach can be used to express the force coefficients measured on the mass, M (i.e.: $f = f_s + f_c$):

$$f_s = K_s d_{33_s} + \frac{K_s v_s}{j\omega} + C_s v_s \quad (4.10)$$

and

$$f_c = 0 + \frac{K_s v_c}{j\omega} + C_s v_c \quad (4.11)$$

With those four coefficients (v_s , v_c , f_s and f_c) the error contributions E_s and E_c can be calculated for different actuator characteristics and for any desired impedance condition Z_d . These various parameters may be varied independently to determine their effect on controllability.

4.2.2 Effect on Controllability

A model of the entire system (Cf: Figure 4.2) can be obtained by substituting values for the variables (K, C, M, d_{33}, \dots). In the following example, both the control and sample actuators have been chosen to be identical. Choosing a junction mass $M=280\text{g}$ and given values for the other coefficients, that gives a new system whose natural frequency is 600Hz . Substituting equations (4.8) through (4.11) into equations (3.8) and (3.9) allows to see how both errors E_c and E_s behave over a range of frequencies for different desired impedance conditions.

It has seen previously, in the limitations of control in Chapter 3, that it is desirable that E_c is never significantly smaller than E_s . If this happens, then the control actuator has to drive very hard in order to achieve the desired impedance condition (i.e.: H becomes large). Figure 4.3 shows the error contributions due to the sample (solid line) and control (dashed line) actuators in four different impedance conditions. In the four different cases, the desired impedance condition is always real (as for the case of a damper) but with a magnitude varying from a low level ($Z_d=.1$) to a high level ($Z_d=10e4$). As one can see with the plots, below the resonant frequency of the system, for all of the different impedance cases, the error level of the control actuator is higher than the error level of the sample actuator. This implies good controllability (the controller will not have to deliver a high control signal). Above the natural frequency of the system, the opposite happens. E_c becomes smaller than E_s and a large input voltage will be required by the control actuator to achieve good control (bring the error, E , to zero). Furthermore, it can be noticed that the difference between the two error terms is more significant for low impedance conditions.

Under high impedance conditions, it is easy to see from equations (3.8) and (3.9) that the terms f_s and f_c become almost insignificant in their contribution to the error. Then, since

the velocity terms, for identical actuators, are the same in magnitude (equation (4.8) and (4.9)) both errors are the same for high impedance conditions ($E_c \approx E_s$): the controllability is good over the entire bandwidth of actuation.

One conclusion that can be made is that to provide good control, it is necessary for the test set-up to have a resonance frequency well above the frequency range of interest.

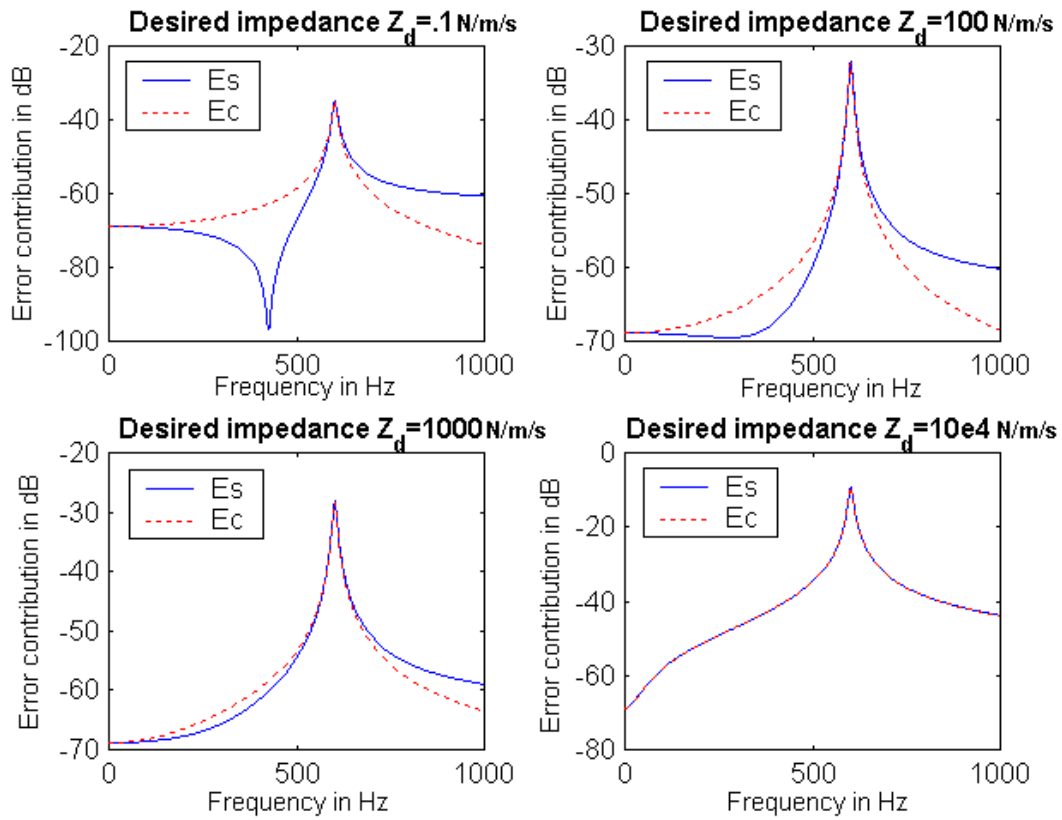


Figure 4.3: Contribution to the error from the sample actuator and the control actuator over various impedance requirements

4.2.3 Effect of Control Actuator Stiffness

To determine the effect of control actuator stiffness on performance, simulations were conducted in which the control actuator stiffness, K_c , was varied. Figure 4.4 shows the importance of making the control actuator stiffer than the sample actuator ($K_c=2*K_s$) since this condition always gives, under the resonant frequency, a smaller error E_s , compared to E_c . This should, therefore, provide better control. On the contrary, when $K_c=0.5*K_s$ (Cf: Figure 4.5), it can be seen that the error E_c is always smaller than the error E_s . This difference between the control and the sample actuator will automatically lead to control authority problems. This can be easily understood since, for a piezoelectric actuator, stiffness and blocked force are directly proportional (Cf: equation (1.1)). Therefore, the actuator with higher stiffness will have the higher force output. Because of this relationship between force and stiffness, the actuator with greater stiffness will have a greater control capability compared to the other one. This explains why it is important for the control actuator to be the one with the greater stiffness.

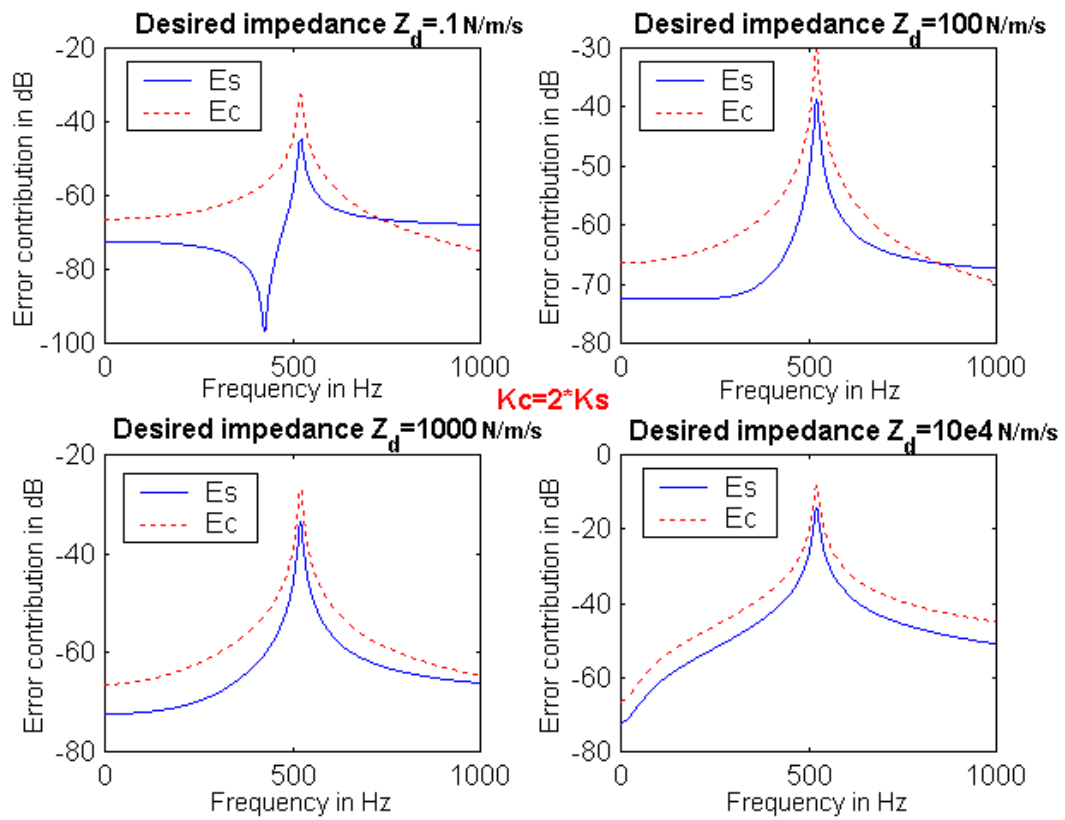


Figure 4.4: Contribution to the error from the sample actuator and the control actuator when $K_c = 2 * K_s$

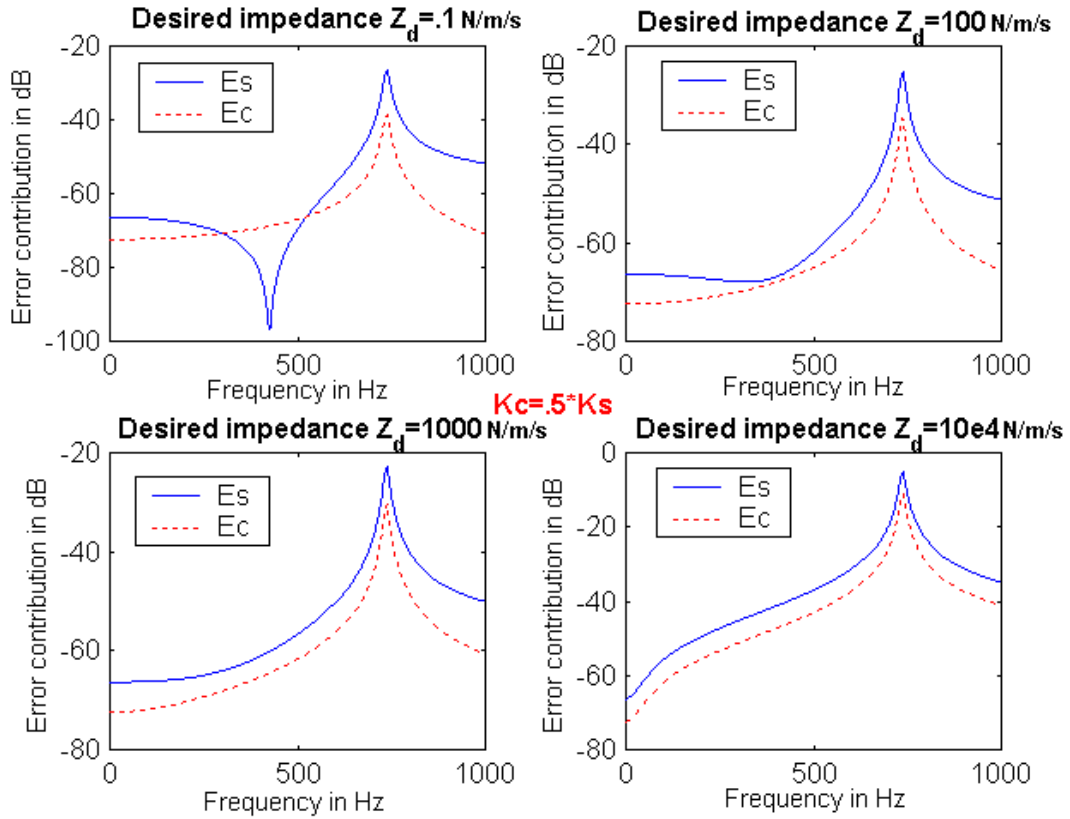


Figure 4.5: Contribution to the error from the sample actuator and the control actuator when $K_c = 0.5 \cdot K_s$

4.3 Simulation Using Measured Data

4.3.1 Experimental Rig

Having a better idea about the control limitations, an experimental rig was built. The rig shown in figure 4.6 has been designed to be sufficiently stiff compared to the actuators used, in order to prevent resonances of the test rig from being within the

bandwidth of control. The frame is composed of 2 steel rods (length: 8 inches, diameter: 7/8 inch) on the sides, 2 aluminum plates (Length: 5.5 inches, height: 1 inch), one shorter steel rod on the middle to ensure a static compressive load (not necessary with the PCB's actuators used in the first experiments).

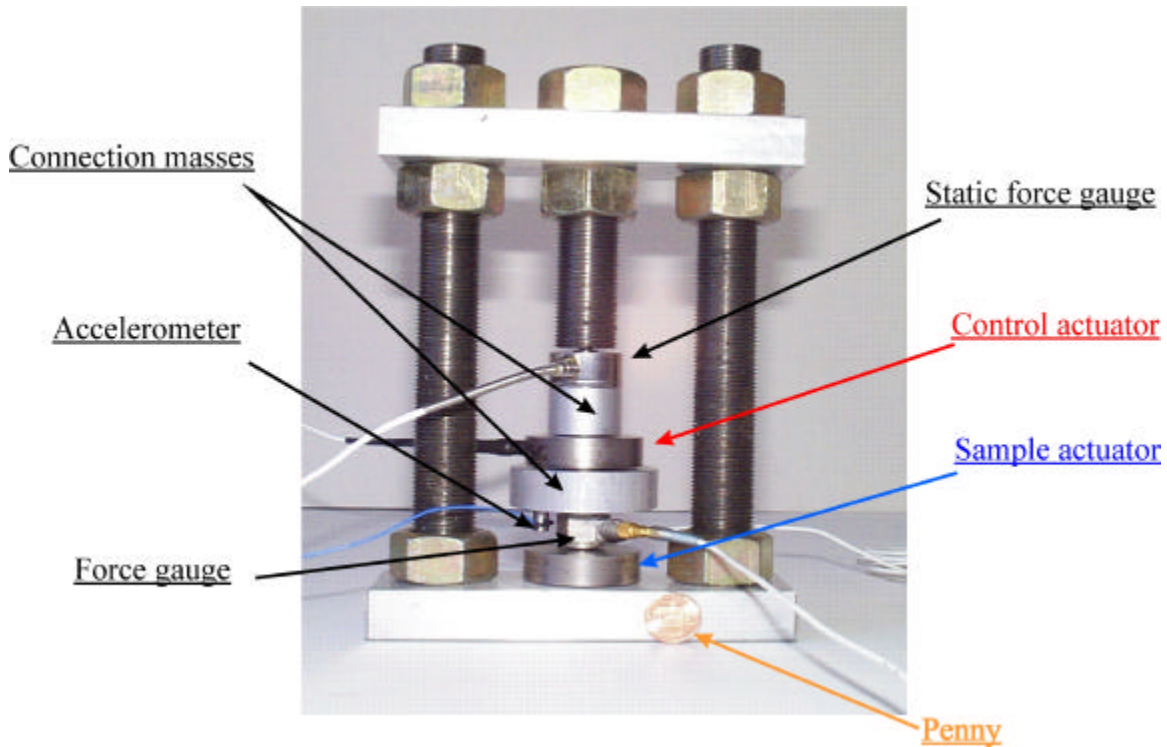


Figure 4.6: Experimental rig showing the two actuators connected in series via a force gauge.

The sample and control actuators used on this rig are flextensional actuators model 710MO2 from PCB (these devices were chosen mainly for convenience and will be later substituted with the 1_3 tube array piezoelectric actuators provided by MSI). A static load cell (model 31/1432-07 from Sensotec) is included in the test set-up so that the static pressure could be monitored. As the PCB's actuators do not require any compressive load, the pressure applied with the middle rod will be kept to a minimum in this case. The dynamic force transducer, model 208A03, and the accelerometer, model 309A,

which were used on the set-up to measure the force and velocity signals, respectively, are shown on Figure 4.7. They were also sensing devices from PCB.

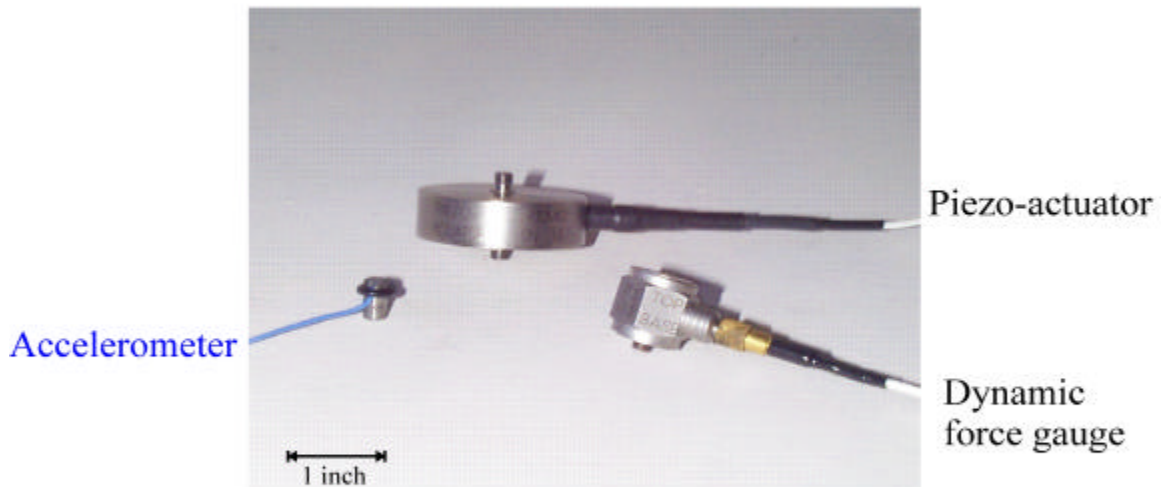


Figure 4.7: Main devices used on the test rig

To ensure that the frame of the test rig was sufficiently rigid, the vibration levels at five positions on the rig were monitored while the control actuator was driven with white noise. The control actuator was chosen over the sample actuator since it generates the highest level of excitation on the rig. These positions are shown in Figure 4.8. Despite a resonant frequency around 900Hz, the vibration of the center mass was more than 40dB larger than the vibration at all of the others positions for a frequency range of interest from 0 to 1600Hz.

Therefore it was concluded that, for these actuators, the test rig was sufficiently rigid and the base had a large enough input impedance. It was important to fulfill this requirement

since it met the original assumption of no displacement of the bottom side of the sample actuator. Knowing the test structure modal character to be appropriate for the bandwidth of control, actuator characterization tests could then be conducted.

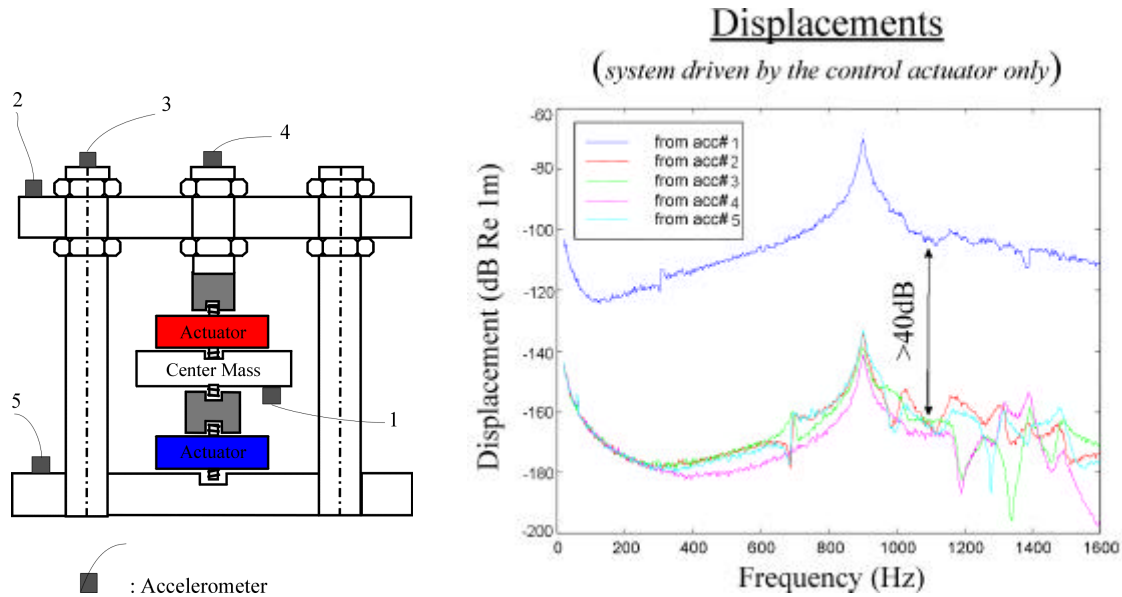


Figure 4.8: Transfer functions of the displacement on the rig when the control actuator is driven with white noise

4.3.2 Application of the Simulation

To test the methodology, a control simulation for an easily reproducible case was conducted. The desired impedance was set to be the one of a 100g mass (i.e.: $Z_d = j\omega 0.1$, where j is such that $j^2 = -1$ and ω is the frequency in rad/s). Using measured data, the goal was then to simulate the behavior of an inertial actuator with a 100g inertial mass. The results could then be compared with the performance of a real inertial actuator with a 100g inertial mass.

To achieve this, the four transfer functions of the force and velocity in both cases where the control and the sample actuators are driven separately were measured, $F_c=f_c/s_c$, $V_c=v_c/s_c$, $F_s=f_s/s_s$ and $V_s=v_s/s_s$ respectively. After using these four transfer functions to compute the transfer functions of the different impedances, $Z_s= f_s/s_s*s_s/v_s$ and $Z_c= f_c/s_c*s_c/v_c$, and setting the desired impedance as the one of that 100g mass, the control filter, H (equation (3.10)), could then be easily calculated. Figure 4.9 explains the principle of this simulation technique.

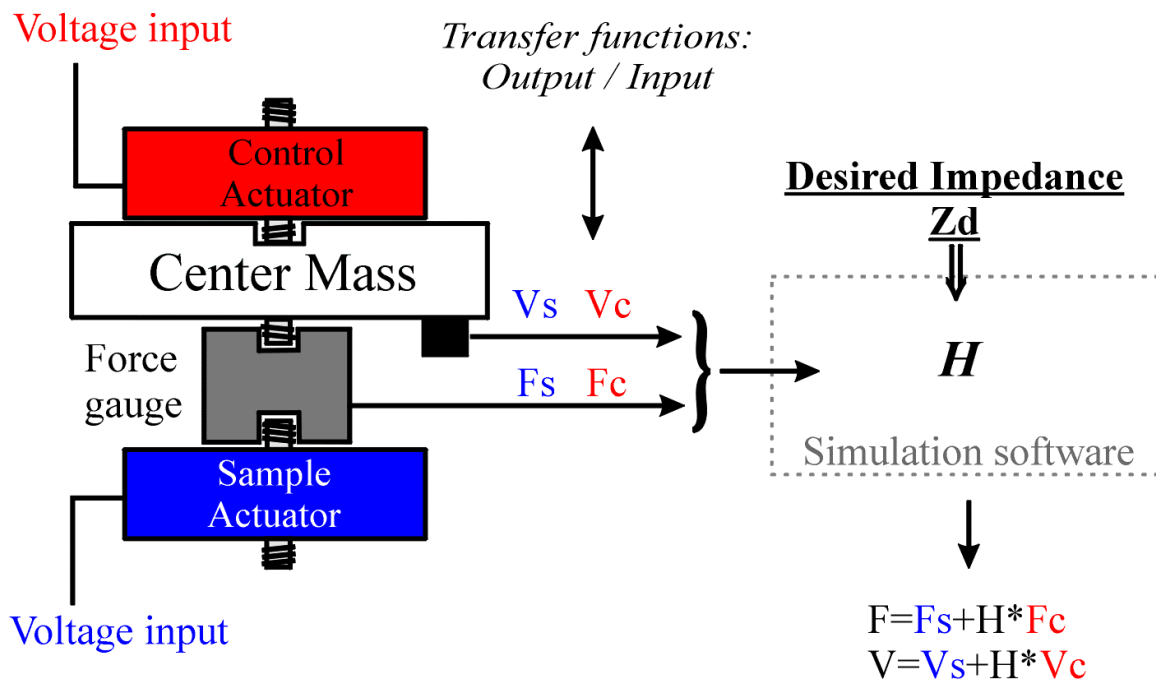


Figure 4.9: Principle of the control simulation using measured data

This simulation was used to compare predicted performance with a measured impedance from a real load. This comparison would then reveal some limitations that controller might encounter later. In the experimental case the force produced by this inertial actuator was measured under an actuator shaking a 100g mass (Cf: Figure 4.10, drawing on the top left). For the simulation, a force gauge on the base of test rig under the sample

actuator was used to monitor the actuator force output (Cf: Figure 4.10, picture on the bottom left). This extra force gauge (that was not mount on the initial test rig (Figure 4.6)) was necessary to get the measurements of a comparable force that the one measured in the experimental case. Two additional transfer functions between the inputs to the actuators and the force input to the base of the test rig were measured (f_{bs} and f_{bc}) and using the principle of superposition the total force input to the base of the test rig could then be calculated as:

$$F_t = (f_{bs} + H.f_{bc}).s_s \quad (4.9)$$

This method is shown in Figure 4.9. The total force calculated using this method is an estimate of the force that would be created at the base of the rig if the controller were simulating the behavior of a 100g load. Figure 4.10 compares this force with the force measured using an actual 100g load on the sample actuator. For the force to be accurately modeled, certain adjustments had to be made. First, part of the mass of the force gauge (about half of it) is already included in the measured force output for the real inertial actuator. The measured data for the transfer function of the force (f_c and f_s) correspond then to an inertial actuator with a little higher mass (approximately 115g which is equal to the 100g mass plus around 15g due to the mass of the force gauge itself). This explains why using this data, the simulation predicts a lower natural frequency than the one measured on the experimental set up (Figure 4.10). To adjust for this, an 85g load was chosen as the desired impedance, taking the pre-existing 15g due to the force gauge into account in the simulation. With this adjustment, both natural frequencies of the inertial actuator and the simulation matched very well.

A second adjustment was required because of a phase matching problem between the force gauge and the accelerometer. For a lightly damped resonance condition only a few degrees of phase mismatch can transform a reactive impedance (i.e.: a mass or a spring) into a significant real impedance (i.e.: damping). This accounts for the damped resonance condition predicted using the simulation (Figure 4.10). It appears then, that the sensor devices measuring both force and velocity have to be perfectly phase matched to

ensure a perfect measure of the impedance. As a complex value, the measure of the impedance requires a good precision not only of its magnitude but also of its phase. Therefore, to ensure good control those phase mismatches also have to be compensated. After these effects (mass and phase) were accounted for, the force predicted using measured data from the rig and measured force from the real inertial actuator matched very well (Cf: Figure 4.10, dashed plot).

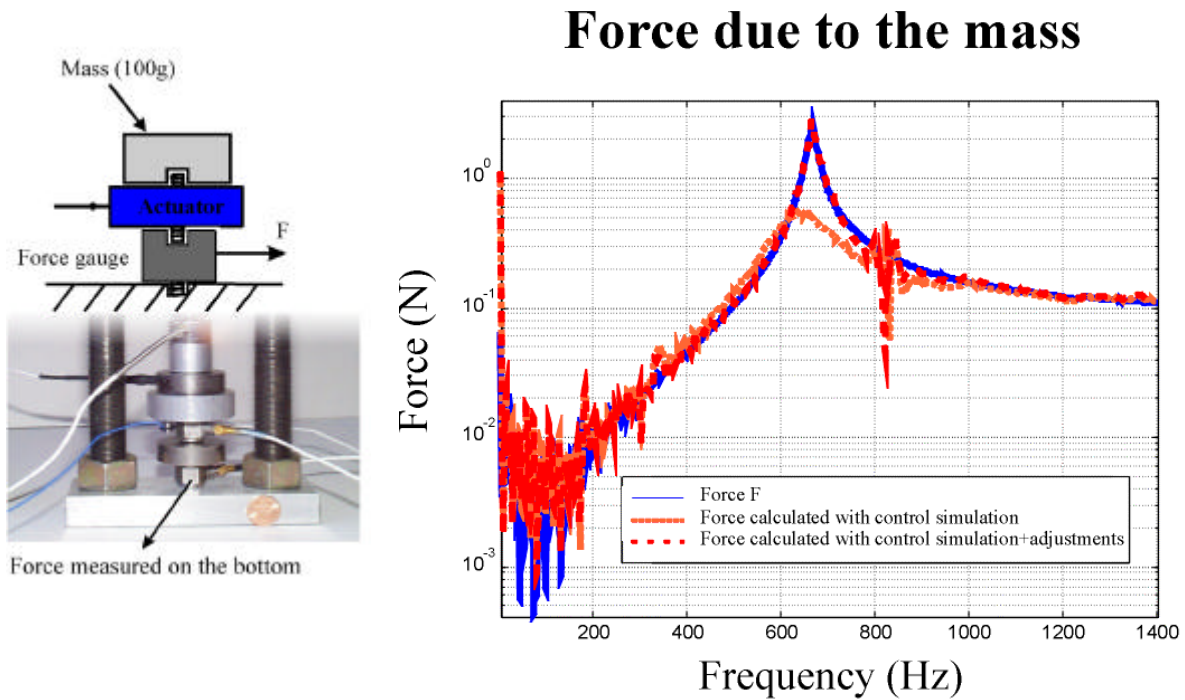


Figure 4.10: Comparison between the force out of an inertial actuator and the one obtained with control simulation for the corresponding desired impedance

4.4 Conclusion

At this point of the research, all the methodology to create a test set-up, which would allow the user to simulate a wide range of load impedances and to assess the performance of the actuator under these conditions, has been developed and tested through various simulations. Some practical limitations due mainly to control authority, resonant frequencies of the system and measurement accuracy due to the sensor devices themselves (problems of phase mismatch) have been raised. However these limitations do not look totally insurmountable and they should easily be overcome making improvements to the rig. Therefore, the next stage is to develop the real time DSP (Digital Signal Processing) software that would allow to perform the active feedforward control of impedance (Cf: Chapter 5).